Forecasting tropical ENSO-induced drought conditions using sea surface height in the Western Pacific

Carlos Primo David
University of the Philippines
Manuel Justin Custado
University of the Philippines
Natasha Sekhon
Brown University
Daniel Ibarra (daniel_ibarra@brown.edu)
Brown University https://orcid.org/0000-0002-9980-4599

Article

Keywords: sea surface height, drought, El Niño Southern Oscillation, Sea surface temperature

Posted Date: September 22nd, 2021

DOI: https://doi.org/10.21203/rs.3.rs-926783/v1

Forecasting tropical ENSO-induced drought conditions using sea surface height in the Western Pacific

C.P. David[1], M.J. Custado [1], N. Sekhon[2,3], D.E. Ibarra[2,3*]

[1] National Institute of Geological Sciences, University of the Philippines Diliman, Quezon City, Philippines

[2] Department of Earth, Environmental, and Planetary Sciences, Brown University, Providence RI, USA

[3] Institute at Brown for Environment and Society, Brown University, Providence RI, USA

*Corresponding author: daniel_ibarra@brown.edu

Abstract

The interannual variability of rainfall caused by the El Niño Southern Oscillation (ENSO) results in significant changes in hydrologic conditions that affect entire countries' water supply. Forecasting ENSO and its impacts are mainly based on Central Pacific Sea surface temperature (SST) anomalies which satisfactorily correlates with timing and, to a lesser extent, the intensity of drought conditions in the Philippines and the rest of the Western Pacific during the El Niño phase. Changes in sea surface height (SSH) are also brought upon by ENSO through density changes with temperature and oceanographic processes. Here, we report that the associative nature of SSH and drought as measured by surface runoff, has a stronger correlation ($r > 0.693$, $p < 0.05$) in terms of the expected timing, with 1 to 3 months lag time, and intensity compared to using traditional ENSO SST indices from the Central Pacific. Furthermore, since SSH is co-located with its corresponding forecasted decrease in runoff, a localized prediction can be made which further increases the accuracy of this predictive tool. In the wake of a changing climate, this work demonstrates the possibility of statistically forecasting the timing of precipitation, and thus the volume of surface water availability, using local SSH as an indicator. A tool which is necessary for time-sensitive management decision making in drought-prone tropical regions.

Main

The El Niño Southern Oscillation (ENSO) results in significant deviations in continental precipitation primarily in the Eastern Pacific but its effects on the water cycle are felt via atmosphere-ocean teleconnections across the globe[1]. ENSO is triggered by sea surface temperature (SST) anomalies emanating from the Central and Eastern Pacific and is primarily used to predict the ensuing ENSO impacts. Significant work has been done in fine tuning SST-based indicators

such as constraining the region of warming, resulting in the identification of the Nino Index Regions[2] and the development of the Oceanic Nino Index (ONI)[3]. Further, the recognition of different ENSO "flavors" has led to the development of other indices[4], the use of dynamic ocean/atmosphere coupled models[5,6] and improved data calculation and interpolation techniques[7,8] in order to extend and potentially improve the accuracy of predictions for impacts associated with ENSO teleconnections. A majority of these improvements are geared towards predicting impacts in the Eastern Pacific; however, research is increasingly focusing on forecasting ENSO impacts in other regions owing to this phenomenon's far-reaching effects on global climate variability on interannual timescales, occurring every two to seven years[9].

Many counter-intervening processes are in operation in the Central and Eastern Pacific, including the timing of the annual cycles of outgoing longwave radiation which affects atmospheric convection and in turn controls the location and intensity of warming in the tropical Pacific[3]. Further, ocean-atmosphere coupled models have also been found to be less accurate in predicting the global SST pattern during weak ENSO events[10]. Similar ocean-atmosphere interactions in the Western Pacific and other parts of the globe may likewise complicate the ensuing ENSO impact in the countries bordering the Western Pacific. Thus, a more localized indicator of interannual variability is required to provide better predictive capabilities for these countries beyond the indices based solely on the Central and Eastern Pacific SST anomalies. In this work we explore such an indicator using sea surface height as a predictive tool for tropical drought as measured by the ensuing decrease in river runoff.

SSH is directly tied to temperature as warm water is less dense than cold water, such that locally higher SSH regions tend to be warmer than lower SSH areas[11,12] coupled with strong eastward Kelvin waves that trap coastal waters in the Eastern Pacific coast[13]. SSH's relationship with temperature led Shi et al.[14] to recently differentiate Central Pacific from Eastern Pacific El Niño types through the development of an SSH-based Index rather than the more traditionally used SST-based indices. Finally, researchers have also previously recognized the strong association between low rainfall conditions and low sea surface height (SSH) in Indonesia[15].

Situated in the equatorial Western Pacific, the Philippine Archipelago is ten thousand kilometers away from the Central Pacific yet extremely affected by ENSO variability, albeit with the reverse sign of what is experienced in the Eastern Pacific. During the El Niño phase, drought conditions are felt across the different islands of the country[15]. SST anomalies generally correlate with drought conditions in the Western Pacific but become less accurate with regards to the onset and expected intensity of drought vis a vis the intensity of ENSO conditions. In fact, the onset of the 2009-2010 moderate intensity El Niño years resulted in extensive rainfall in the Philippines[16], the opposite of the canonically expected sign. This is due to other compounding factors such as the varying rainfall and temperature signatures of each ENSO event and their susceptibility to the hydroclimate character of the preceding years[15]. The decrease in rainfall due to El Niño conditions also varies in magnitude across the country with unpublished data on highest precipitation anomalies being reported to affect the country's eastern seaboard while combined precipitation and temperature anomalies are highest in the middle of the largest Philipipne islands, Luzon and Mindanao. Given the motivating need for a more localized indicator of drought, this paper presents the use of local SSH measurements as a high-resolution indicator of drought conditions across the

Philippine Archipelago in an analogous sense to using ENSO indices for such forecasting. To the best of our knowledge, this is the first time that it is being reported that SSH data is used for localized ESNO-related drought prediction.

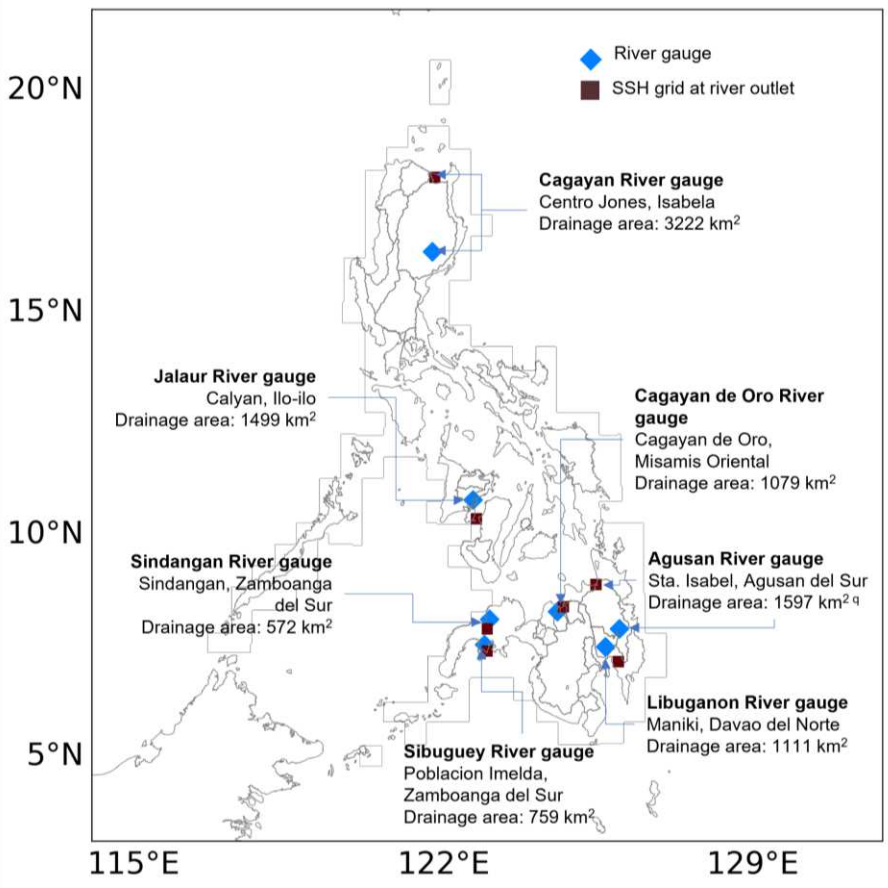

Figure 1. Location of the seven river basins analyzed in this study including where the actual river gauge station is located as well as each river's outlet to the ocean. The thin, gray lines bordering the coastal waters of the country correspond to the spatial overlap of the SSH and GRUN datasets.

River gauge, GRUN and SSH data

A comparison between actual stream gauge data of major rivers in the Philippines with at least ten years of GRUN data is provided in Extended Data Table 1. As reported by Ibarra et al.[17], actual

stream gauge and the global gridded runoff dataset generally show a fair correlation between them which can further be improved upon correction of systematic biases. The same table directly correlates stream gauge data with SSH where the r-value is given for the lag time that showed the highest correlation. Data for SSH also shows high correlation with actual stream gauge data for almost all of the large basins considered. This points to the validity of the two parameters' strong association, and which we then carry over to investigating GRUN-SSH correlations in the below analyses.

National analysis between GRUN and SSH time series

Using the GRUN data, we now correlate river runoff and sea surface height as a national aggregate, regionally and at the basin level. The national annual averages of GRUN and SSH are plotted in Figure 2 where it clearly shows the seasonal cycle of stream runoff including a short dry spell that is usually centered around August every year. A similar but more erratic seasonal cycle is also observed in SSH. Deseasonalizing and detrending the data as shown in the lower figure clearly presents the years with lowest runoff values corresponding well to El Niño years including the two most recent strong El Niño years of 1997-1998 and 2014-2016. The same figure presents the strong association of runoff and SSH with a noticeable time lag during some years. The detrended plot not only shows the similar pattern between the two datasets but also the high association of detrended SSH and runoff values. Again, also evident in Figure 2 are the lowest SSH and runoff values centered on the two strong El Niño events of 1997-98 and 2015-2016. These two events are more than 1.5mm/day lower than mean runoff and about 0.1m lower than mean SSH.

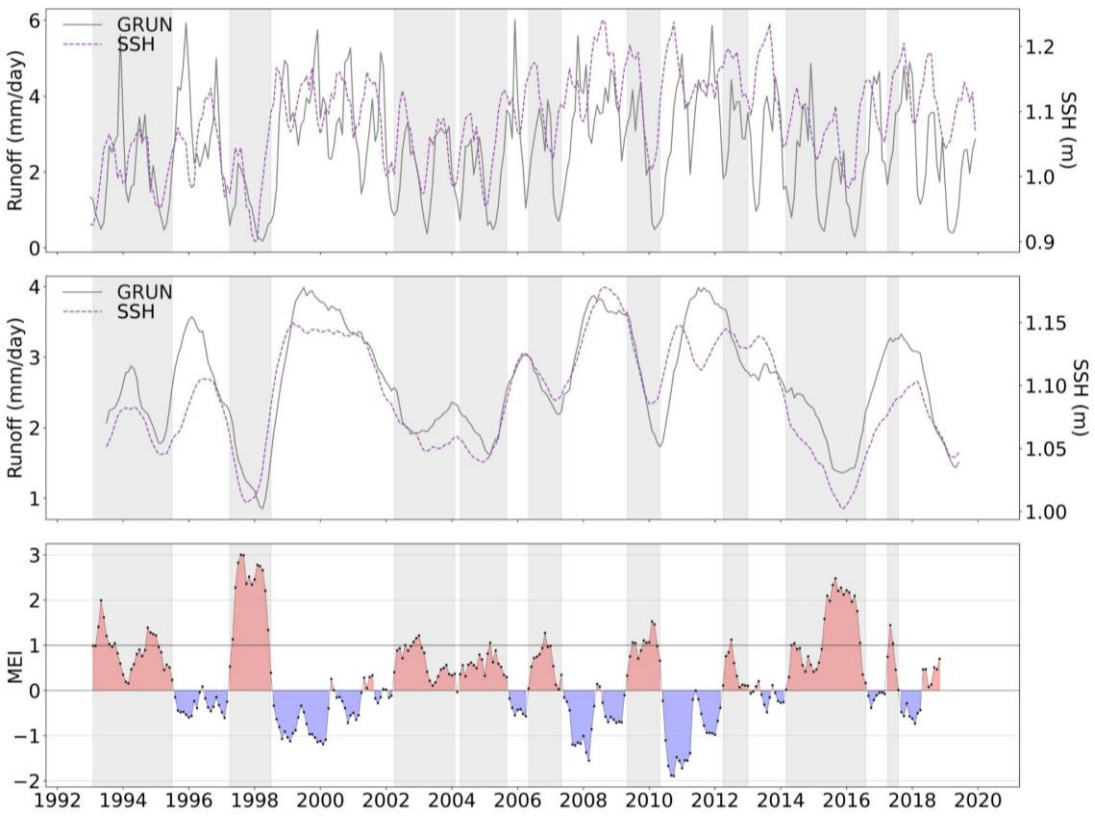

Figure 2. Monthly time series of GRUN and SSH, national means during periods of overlap (1993 - 2019) and the Multivariate ENSO Index (1993 - 2018). Top: monthly time series of GRUN and SSH; middle: deseasonalized and detrended time series of GRUN and SSH; bottom: the MEI. Highlighted time periods (in gray) correspond to the nine relatively strong El Niño events (peak MEI > 1) used in the regression analysis. From left to right, these time periods are: (1) 12/1989 to 07/1995, (2) 04/1997 to 07/1998, (3) 04/2002 to 02/2004, (4) 04/2004 to 09/2005, (5) 05/2006 to 05/2007, (6) 05/2009 to 05/2010, (7) 04/2012 to 01/2013, (8) 03/2014 to 08/2016, and (9) 04/2017 to 08/2017.

Wavelet analyses of the national averages with and without removing the seasonal cycle and detrending shows a one-year periodicity and correlation between SSH and runoff (Figure 3). Further, as shown by the arrows in the wavelet analyses, across the time series SSH consistently

leads runoff nationally. This is supported by the correlation coefficients derived from the two datasets (Extended Data Table 2), as r-values are highest when SSH leads runoff by 1 to 2 months ($r = 0.833 - 0.835$, $p < 0.05$). However, significant correlation between the two parameters still exists even at an SSH lag of 3 months ($r = 0.693$, $p < 0.05$). Extended Data Table 2 also shows that SSH generally correlates with runoff better than SST derived from the Moderate Resolution Imaging Spectroradiometer (MODIS) – Aqua sensor, particularly during positive time lags. Map-view representations of the correlations at several time lags of SSH relative to runoff generally show relatively high r-values across the country (Figure 4). This further suggests the utility of SSH data as a predictor for average runoff levels at the national scale.

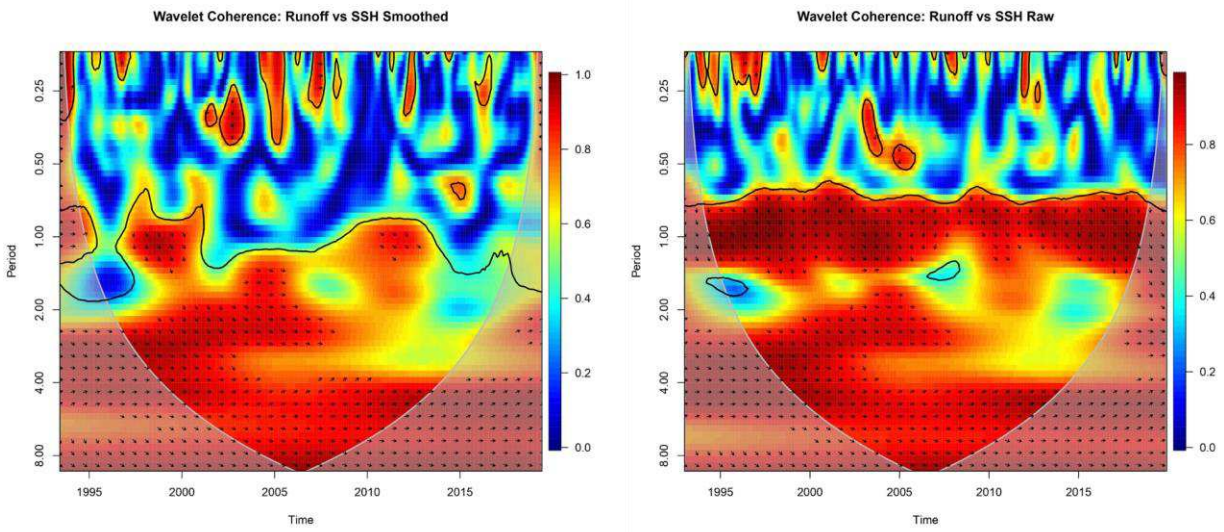

Figure 3. Wavelet coherence plots between runoff and SSH. Direction of arrows indicate time lag; downward direction corresponds to zero time lag, while arrows pointing to the right indicate that SSH leads runoff. Left: Smoothed time series; right: raw time series.

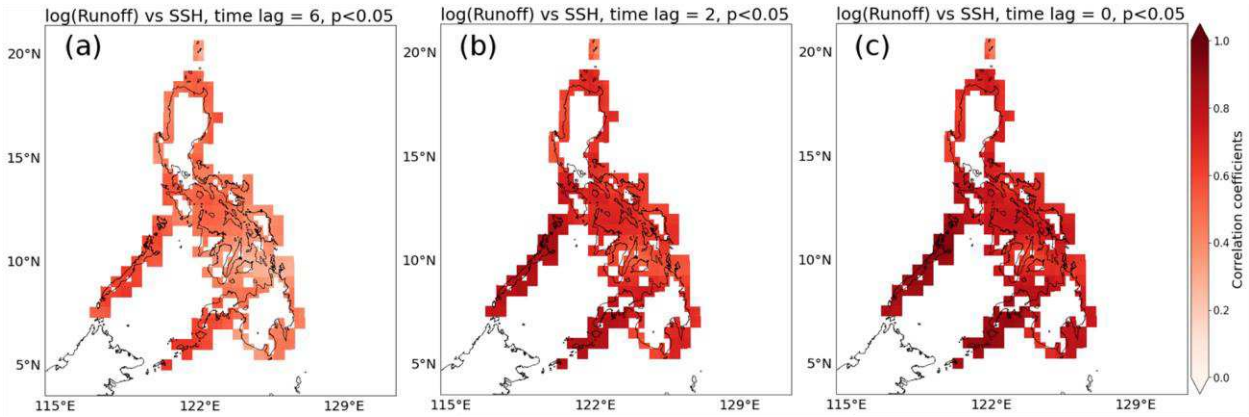

Figure 4. Map of correlation coefficients (1993 - 2019). Left to right: (a) at 6 months that SSH precedes runoff, (b) at 2 months that SSH precedes runoff, (c) at no time lag. Time lag in months.

Region-based analysis of SSH and GRUN

To expand the associative nature of SSH and runoff we further our analysis by grouping coastal areas around the Philippines that show similar SSH versus runoff trends. Nine geographic regions are identified in Figure 5 to have coherent characteristics. An illustration of the calculated correlation coefficients for each region is presented in Figure 6. Interestingly, higher SSH and runoff correlations are found on the western side of the country, particularly in Palawan, and the Zamboanga and Sulu region. The lowest SSH versus runoff correlations are observed in areas directly in contact with the Western Pacific such as northern Luzon (Batanes and Cagayan) and the eastern coast of the country (Eastern Luzon and Eastern Mindanao and Samar).

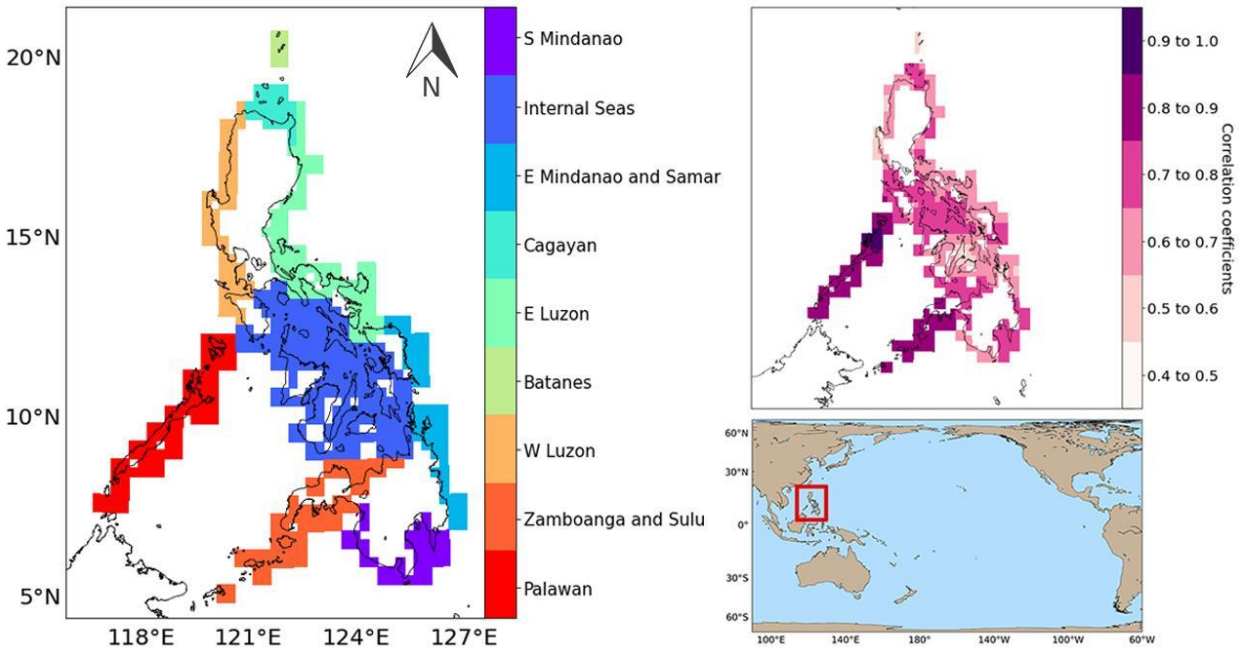

Figure 5. Study area divided per region according to the magnitude of correlation coefficients at -1 month time lag. Right: identified regions; left: reference correlation map at 1 month time lag of SSH and the Pacific Ocean map. Red box indicates the location of the study area.

Other than the different correlation values between SSH and runoff, the time lag with the maximum r-value at each identified region also differs from one another (Figure 6). The regions of Palawan, Zamboanga and Sulu, and Southern Mindanao achieve the highest correlation with r-values of 0.914, 0.900, and 0.813, respectively at time lags from -1 to -3 months. For Southern Mindanao, the highest correlation is achieved at time lag = -3, whereas for the two other regions the time lag with highest correlation is at t = -1. Significant correlations (r = 0.734 to 0.775) are also observed for the rest of the regions at time lags of either t = -1 or -2, except for the northernmost islands of the Batanes region, which attains its highest correlation with no time lag. Presumably, the Batanes region is the least affected by SSH variations as it is already 20 degrees north of the equator.

Runoff estimates from may likewise be off due to the small catchment size of the small, individual islands of the region[17].

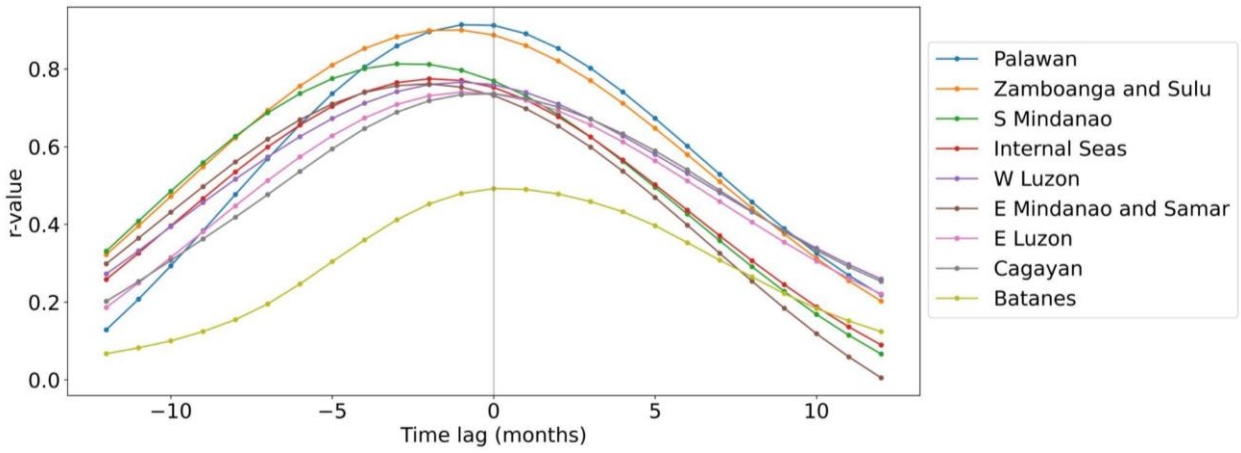

Figure 6. Correlation coefficients between $\log_{10}$(runoff) and SSH at each region from -12 to 12 months of time lag of SSH. The regions are listed in the plot legend according to the magnitude of correlation coefficients calculated; Palawan and Batanes have the highest and lowest peak r-values, respectively. A positive time lag means SSH precedes runoff; a negative time lag means SSH leads runoff. See Supplementary Table 1 for the matrix of values plotted here.

Drought prediction using SSH during positive phase ENSO events

In this section, we discuss ENSO-induced drought and its prediction using SSH. For this, we select significant El Niño events (n = 9) based on the Multivariate ENSO Index (MEI) within the period of overlap between the GRUN and SSH datasets (1993 to 2018) and isolate the minimum runoff and SSH values that correspond to such events. These El Niño events are identified by the time periods with consistent positive MEI and with a maximum value of MEI > 1: (1) 12/1993 to 07/1995, (2) 04/1997 to 07/1998, (3) 04/2002 to 02/2004, (4) 04/2004 to 09/2005, (5) 05/2006 to 05/2007, (6) 05/2009 to 05/2010, (7) 04/2012 to 01/2013, (8) 03/2014 to 08/2016, and (9) 04/2017

to 08/2017. Extended Data Table 3 provides the correlation coefficients which again shows the high association between minimum SSH and minimum runoff during drought conditions for most regions. This is especially true for the western side of Luzon (r = 0.937) and southern Mindanao (r = 0.901) which are the country's largest agricultural lands and regions that are highly susceptible to drought conditions[18]. Extended Data Table 3 shows the time lag wherein SSH can be used as a predictor for minimum runoff during strong El Niño events. Peak correlations range from a 4 month time lag to no lag at all depending on the region.

Given the results from the preceding sections, we propose the future development of an SSH-based drought forecasting tool for water management purposes. First, the MEI or similar ENSO indices is used to determine the background state of the climate system in the Pacific Ocean with a predictive horizon of 6 to 12 months. If the MEI is greater than 0, drought conditions regionally can be forecasted using the prevailing SSH and the SSH vs. runoff regressions presented above within a 2 to 4-month window of the dry season. A nationwide network of SSH gauging stations must be established for real-time analysis to be possible. Based on the historical correlation of SSH and runoff per region, an appropriate range of probable drought levels based on historical and projected runoff data (calculated as a decrease in rainfall for non-irrigated areas) could then be provided per basin in each and every region.

Conclusions

The latest Intergovernmental Panel on Climate Change (IPCC) report[19] concluded that it will be virtually certain that the ENSO will remain the dominant mode of interannual variability for precipitation in a warmer world. Moreover, it is very likely that rainfall variability related to

changes in the strength and spatial extent of ENSO teleconnections will lead to significant changes at regional scale[19]. As such, this is a compelling reason why our predictive capabilities of droughts should be further enhanced. Even with only several months in advance, the accurate prediction of local hydrologic conditions coupled with an effective water management program will allow for climate change adaptation measures to be implemented.

This study highlights the importance of similar predictive tools that are associative in nature and not necessarily causative. The high correlation of SSH and runoff detailed in this study provides an additional tool for ENSO-induced drought prediction with a shorter predictive horizon (2-4 months lead time) but of higher accuracy compared to using the standard central Pacific SST-based tools used to characterize ENSO for global teleconnections. SST anomalies are translated into changes in local SSH values which presumably are affected by other oceanographic factors beyond just SST and subsequentially drive local-scale precipitation and drought conditions. These compounding factors are beyond the scope of this research but may include the seasonal timing of such anomalies, ocean-atmosphere interactions and ocean circulation dynamics. What we presume is that the same factors are also imposed on factors influencing precipitation amount and resulting stream runoff thus leads to the higher correlation between SSH and runoff instead of the causative SST information from the Pacific Ocean basin. This inference is useful for the development of a drought forecasting tool associated with El Niño events with greater accuracy and skill.

Methods

Data

The primary data used for this study were monthly composites of SSH and runoff from satellite altimetry records and the GRUN Ensemble dataset, respectively. Drought is herein quantified based on stream discharge, in particular the amount of decrease in the minimum observed flow in rivers. In the following sections, we introduce the origin and data handling of these datasets.

Satellite altimetry data

Daily level-4 SSH products with a spatial resolution of 0.25° (~27 km) were retrieved from the Copernicus Marine Environmental Monitoring Service (CMEMS) database. These datasets are the products of the most recent version of the Data Unification and Altimeter Combination System – delayed time (DUACS DT2018), implemented since April 2018 to produce merged datasets of all available satellite altimeter missions globally. The altimetry data products were routinely processed and distributed by Aviso from 2003 to 2017 and by the European Copernicus Program since 2015[20]. Sea surface height measurements from the datasets refer to the absolute dynamic topography (ADT), which is the SSH above the reference geoid.

The DUACS system has continuously been assessed at regional scales by comparing processed sea level anomaly (SLA) data against independent along-track missions and tide gauge data[20]. Overall improvements in the DT2018 products from the DT2014 version were observed using a tide gauges network in the Mediterranean Sea[20]. Ruiz-Etcheverry et al.[21] saw good comparisons between tide gauge data and gridded SLA globally, with root-mean-square differences lower than 2 cm for 76% of the sites studied. Larger error values between tide gauges and satellite altimetry

are accounted for by factors such as nearby river discharge (e.g. Ganges River), currents, seasonal sea ice, and large distance between the gauges and regions with dense along-track altimetry data (e.g. Gulf of Thailand and Panama Bay). Sea level errors were quantified at the mesoscale range from 1.4 cm^2 to 30 cm^2 from low to high variability areas[20]. Independent assessments of altimetry data saw global bias estimates from each satellite mission[22,23]. In previous works, satellite altimetry data have shown great utility in various sea level applications across different study sites, such as the Palau Islands, Malaysia, West Philippine Sea, and Argentina[24-27].

GRUN Ensemble

The GRUN Ensemble dataset is a global runoff product derived from a machine learning algorithm trained using streamflow observations from the Global Streamflow Indices and Metadata Archive (GSIM). It has a spatial resolution of 0.5° (~ 55 km) spanning from 1901 to 2019. Only discharge data from catchment basins with areas between 10 and 2,500 km^2 were used as training input to the algorithm[28,29]. This version of the GRUN dataset[28] improves upon the first iteration[29] by using temperature and precipitation data from an ensemble of 21 global datasets as input to the developed algorithm. Validation of the runoff product utilized discharge data from basins with more than 10,000 km^2 of area and its accuracy was assessed against nine other global hydrological models[28].

One of the earliest local-scale validations of the GRUN algorithm was conducted by Ibarra et al.[17] by comparing the original version of the runoff product against discharge gauges across the Philippines. They found reasonable utility in the $\log_{10}$-transformed data at the country scale, which further improves when a nationwide bias correction derived from the river gauge comparison is applied.

283

284 ***River gauge data***

285 The Philippines has daily stream gauge data for more than 100 rivers with gauging programs
286 starting as early as the turn of the 20th Century[30]. Unfortunately, like in many other countries, most
287 gauging data are not continuous and thus we use the global GRUN dataset as a proxy for
288 streamflow. For this study, stream gauging data of seven of the 18 major river basins of the country
289 were selected on the basis of location, period of the gauging data available, and the size of the
290 drainage basin area (Figure 1). These were directly compared to SSH values of the grid overlapping
291 with each of the rivers' outlet to the ocean as a verification of our methods.

292

293 ***Data pre-processing***

294 The GRUN data files were transformed to 0.25° x 0.25° spatial resolution using the conservative
295 nearest-neighbor interpolation method to match with the retrieved SSH data. Daily SSH data were
296 averaged to obtain monthly composites. All the data were spliced to an area bounded by 3.125 to
297 22.125°N and 114.125 to 131.875°E. River gauge data were converted from liters/second to
298 mm/day to match with the GRUN dataset using the basin areas reported in Ibarra et al.[17].

299

300 ***Data analysis***

301 The runoff dataset was $\log_{10}$-transformed following Ibarra et al.[17] based on their comparison to the
302 original version of GRUN, while the SSH dataset was not normalized or $\log_{10}$-transformed. We do
303 this because runoff values vary by several orders of magnitude and represent heavy tailed
304 distributions while SSH values only vary by a small amount (~37%).

305

In order to minimize the influence of seasonal cycles and long-term linear trends, all datasets were deseasonalized and detrended prior to correlation analysis. The seasonality was removed by taking the 12-month centered moving average of each time series. Afterwards, linear regression was applied to each time series to obtain the corresponding linear trend, represented by the resulting equation of the line. The linear trends were then subtracted from the deseasonalized data to obtain the detrended time-series datasets.

Linear correlation analysis was implemented on all the grids within the spatial and temporal overlaps of the data (1993 to 2019, n = 312) at -12 to 12-month time lag/time ahead relative to SSH. Streamflow values were $\log_{10}$-transformed and correlated with the SSH grid at the discharge site of the drainage basins where the gauges are located. Figure 1 shows the location of the river gauge and corresponding gauges in seven of the major river basins of the country. It also shows the actual coverage of the SSH and GRUN grid used in this study.

Data availability

All datasets are available from the papers cited in the above methods and are available in the code package provided with the paper.

Code availability

All python code is provided in a code package (zip file) associated with submission and is available as a Google Colaboratory Notebook linked in the Readme file.

Acknowledgements

We acknowledge a 2019 DOST-PCIEERD Balik Scientist award to DEI and CPD which initiated the collaboration and Pamela Louise M. Tolentino and Mart Geronia for discussions and help with dataset curation. NS is funded by Voss Postdoctoral Research Associate and Presidential Diversity Postdoctoral Fellowships from Brown University.

Author Information

Affiliations

National Institute of Geological Sciences, University of the Philippines Diliman, Quezon City, Philippines

C.P. David and M.J. Custado

Department of Earth, Environmental, and Planetary Sciences, Brown University, Providence RI, USA and Institute at Brown for Environment and Society, Brown University, Providence RI, USA

D.E. Ibarra and N. Sekhon

Contributions

CPD, DEI and MJC designed the study. MJC, DEI and NS conducted the analysis. MJC and CPD wrote the initial manuscript draft. MJC and DEI produced the figures. All authors contributed to the interpretation of the results and to editing the manuscript.

Corresponding author

Correspondence to D.E. Ibarra.

Ethics declarations

Competing interests

The authors declare no competing interests.

355 **References**

356 [1] Kousky, V.E., Kagano, M.T., and Cavalcanti, I.F.A. A Review of the Southern Oscillation:
357 Oceanic-Atmospheric Circulation Changes and Related Rainfall Anomalies. *Tellus A* 36A
358 (5), 490–504 (1984).

359 [2] Rasmusson, E.M. and Carpenter, T.H. Variations in Tropical Sea Surface Temperature and
360 Surface Wind Fields Associated with the Southern Oscillation/El Niño. *Monthly Weather*
361 *Review* 110 (5), 354–384 (1982).

362 [3] Trenberth, K.E. The Definition of El Niño. *Bulletin of the American Meteorological Society* 78
363 (12), 2771–2777 (1997).

364 [4] Trenberth, K.E. and Stepaniak, D.P. Indices of El Niño Evolution. *Journal of Climate* 14 (8),
365 1697–1701 (2001).

366 [5] Tozuka, T. and Yamagata, T. Annual ENSO. *Journal of Physical Oceanography* 33 (8), 1564–
367 1578 (2003).

368 [6] Wengel, C., Lee, SS., Stuecker, M.F. *et al.* Future high-resolution El Niño/Southern Oscillation
369 dynamics. *Nat. Clim. Chang.* **11,** 758–765 (2021).

370 [7] Kirtman, B.P. The COLA Anomaly Coupled Model: Ensemble ENSO Prediction. *Monthly*
371 *Weather Review* 131 (10), 2324–2341 (2003).

372 [8] Zambrano Mera, Y.E., Rivadeneira Vera, J.F., and Pérez-Martín, M.Á. Linking El Niño
373 Southern Oscillation for Early Drought Detection in Tropical Climates: The Ecuadorian
374 Coast. *Science of The Total Environment* 643, 193–207 (2018).

375 [9] Sarachik, E.S. and Cane, M.A. *The El Niño-Southern Oscillation Phenomenon*. (Cambridge
376 University Press, 2010).

377 [10] Sohn, S.J., Tam, C.Y., and Jeong, H.I. How Do the Strength and Type of ENSO Affect SST

Predictability in Coupled Models. *Scientific Reports* 6, 1–8 (2016).

[11] Casey, K.S. and Adamec, D. Sea Surface Temperature and Sea Surface Height Variavility in the North Pacific Ocean from 1993 to 1999. *Journal of Geophysical Research C: Oceans* 107 (8), 14–1 (2002).

[12] Jones, M.S., Allen, M., Guymer, T., and Sounders, M. Correlations between Altimetric Sea Surface Height and Radiometric Sea Surface Temperature in the South Atlantic. *Journal of Geophysical Rsearch Oceans* 103, 8073–8087 (1998).

[13] Nezlin, N.P. and McWilliams, J.C. Satellite Data, Empirical Orthogonal Functions, and the 1997–1998 El Niño off California. *Remote Sensing of Environment* 84 (2), 234–254 (2003).

[14] Shi, J., Fedorov, A. V., & Hu, S. A sea surface height perspective on El Niño diversity, ocean energetics, and energy damping rates. *Geophysical Research Letters*, 47(7), e2019GL086742 (2020).

[15] Harger, J.R.E. ENSO Variations and Drought Occurrence in Indonesia and the Philippines. *Atmospheric Environment* 29 (16), 1943–1955 (1995).

[16] Yumul, G.P., Dimalanta, C.B., Servando, N.T., and Hilario, F.D. El Niño Southern Oscillation in the Context of Climate Uncertainty: The Philippine Setting. *Philippine Journal of Science* 139 (1), 119-126 (2010).

[17] Ibarra, D. E., David, C. P. C., & Tolentino, P. L. M. Evaluation and bias correction of an observation-based global runoff dataset using streamflow observations from small tropical catchments in the Philippines. *Hydrology and Earth System Sciences*, 25(5), 2805-2820 (2021).

[18] Rojas, O. Agricultural extreme drought assessment at global level using the FAO-Agricultural Stress Index System (ASIS). *Weather and Climate Extremes*, 27, 100184 (2020).

[19] IPCC, 2021: Climate Change 2021: The Physical Science Basis. Contribution of Working Group I to the Sixth Assessment Report of the Intergovernmental Panel on Climate Change [Masson-Delmotte, V., P. Zhai, A. Pirani, S.L. Connors, C. Péan, S. Berger, N. Caud, Y. Chen, L. Goldfarb, M.I. Gomis, M. Huang, K. Leitzell, E. Lonnoy, J.B.R. Matthews, T.K. Maycock, T. Waterfield, O. Yelekçi, R. Yu, and B. Zhou (eds.)]. (Cambridge University Press, 2021)

[20] Taburet, G., Sanchez-Roman, A., Ballarotta, M., Pujol, M.I., Legeais, J.F., Fournier, F., Faugere, Y., and Dibarboure, G. DUACS DT2018: 25 Years of Reprocessed Sea Level Altimetry Products. *Ocean Science* 15 (5), 1207–1224 (2019).

[21] Ruiz Etcheverry, L. R., Saraceno, M., Piola, A. R., Valladeau, G., & Möller, O. O. A comparison of the annual cycle of sea level in coastal areas from gridded satellite altimetry and tide gauges. *Continental shelf research*, 92, 87-97 (2015).

[22] Bosch, W., Dettmering, D., and Schwatke, C. Multi-Mission Cross-Calibration of Satellite Altimeters : Constructing a Long-Term Data Record for Global and Regional Sea Level Change Studies. *Remote Sensing* 6 (3), 2255–2281 (2014).

[23] Watson, C.S., Legresy, B., and King, M.A. 'On the Uncertainty Associated with Validating the Global Mean Sea Level Climate Record'. *Advances in Space Research* 68 (2), 487–495 (2021).

[24] Amiruddin, A.M., Haigh, I.D., Tsimplis, M.N., Calafat, F.M., and Dangendorf, S. The Seasonal Cycle and Variability of Sea Level in the South China Sea. *Journal of Geophysical Research: Oceans* 120 (8), 5490-5513 (2015).

[25] Andres, M., Musgrave, R.C., Rudnick, D.L., Zeiden, K.L., Peacock, T., and Park, J.H. On the Predictability of Sea Surface Height around Palau. *Journal of Physical Oceanography* 50

(11), 3267–3294 (2020).

[26] Lago, L.S., Saraceno, M., Ruiz-Etcheverry, L.A., Passaro, M., Oreiro, F.A., Donofrio, E.E., and Gonzalez, R.A. Improved Sea Surface Height from Satellite Altimetry in Coastal Zones: A Case Study in Southern Patagonia. *IEEE Journal of Selected Topics in Applied Earth Observations and Remote Sensing* 10 (8), 3493–3503 (2017).

[27] Luu, Q.H., Tkalich, P., and Tay, T.W. Sea Level Trend and Variability around Peninsular Malaysia. *Ocean Science* 11 (4), 617–628 (2015).

[28] Ghiggi, G., Humphrey, V., Seneviratne, S.I., and Gudmundsson, L. G-RUN ENSEMBLE : A Multi-Forcing Observation-Based Global Runoff Reanalysis. *Water Resources Research* 57 (5), 1–13 (2021).

[29] Ghiggi, G., Humphrey, V., Seneviratne, S.I., and Gudmundsson, L. GRUN: An Observations-Based Global Gridded Runoff Dataset from 1902 to 2014. *Earth System Science Data* 11 (4), 1655-1674 (2019).

[30] Tolentino, P.L.M., Poortinga, A., Kanamaru, H., Keesstra, S., Maroulis, J., David, C.P.C., and Ritsema, C.J. Projected Impact of Climate Change on Hydrological Regimes in the Philippines. *PLoS ONE* 11 (10), e0163941 (2016).

Extended Data Table 1. Correlation coefficients (r-value) of log_{10}-transformed river gauge data with the corresponding log_{10}-transformed GRUN and raw SSH data. The GRUN data analyzed are within the grids where the river gauges are located. The time lag indicated in the correlation with SSH refers to the time lag in months of SSH with the highest r-value. A positive time lag means SSH precedes runoff; a negative time lag means SSH leads runoff.

River	**Period covered of analysis (mm/yyyy)**	**Correlation with GRUN** (r-value, $p < 0.05$)	**Correlation with SSH**	
			r-value ($p<0.05$)	**Time lag** *(months, with respect to runoff)*
Agusan River	01/1993 - 12/2009	0.603	0.711	-2
Cagayan River	01/1993 - 12/2012	0.859	0.747	0
Jalaur River	01/1993 - 12/2010	0.858	0.844	-1
Libuganon River	10/2000 - 12/2009	0.627	0.389	0
Cagayan de Oro River	01/1993 - 12/2004	0.719	0.536	0
Sibuguey River	01/1993 - 12/2010	0.827	0.738	0
Sindangan River	01/1993 - 12/2010	0.785	0.831	-1

Extended Data Table 2. Correlation coefficient values of national means, log GRUN vs. SSH and SST at each time lag relative to SSH and SST. A positive time lag means SSH or SST precedes runoff; a negative time lag means SSH or SST leads runoff.

Time lag *(months, SSH/SST with respect to runoff)*	log GRUN vs SSH (1993 - 2019) r-value, $p < 0.05$	log GRUN vs SST (2002 - 2019) r-value, $p < 0.05$
-8	0.570	0.689
-7	0.638	0.721
-6	0.699	0.734
-5	0.752	0.729
-4	0.793	0.707
-3	0.821	0.667
-2	0.835	0.612
-1	0.833	0.543
0	0.817	0.463
1	0.787	0.375
2	0.745	0.287
3	0.693	0.203

Extended Data Table 3. Correlation coefficients (r-value) between the minimum GRUN during each strong El Niño event and the SSH value at different time lags relative to the minimum GRUN. Highlighted values are the maximum for each region across different time lags. The last row, labeled "Min. SSH", corresponds to the r-value between the minimum GRUN and the minimum SSH during each strong El Niño event, regardless of time lag.

Time lag (months)	Palawan	Zamboanga and Sulu	W Luzon	Batanes	E Luzon	Cagayan	E Mindanao and Samar	Internal Seas	S Mindanao
-6	0.560	0.762	0.508	-0.062	0.321	0.246	0.509	0.638	0.728
-5	0.608	0.766	0.682	0.245	0.618	0.616	0.631	0.830	0.724
-4	0.782	0.683	0.841	-0.035	0.663	**0.772**	0.700	0.835	0.706
-3	0.690	0.806	0.843	0.266	0.776	0.712	0.750	0.806	**0.766**
-2	0.814	0.846	0.909	**0.711**	**0.783**	0.630	0.807	**0.840**	0.754
-1	0.899	0.899	0.880	0.534	0.745	0.545	0.850	0.728	0.724
0	**0.924**	**0.931**	**0.912**	0.558	0.694	0.492	0.**878**	0.623	0.781
Min. SSH	0.878	0.914	0.937	0.574	0.828	0.832	0.824	0.862	0.901

Figures

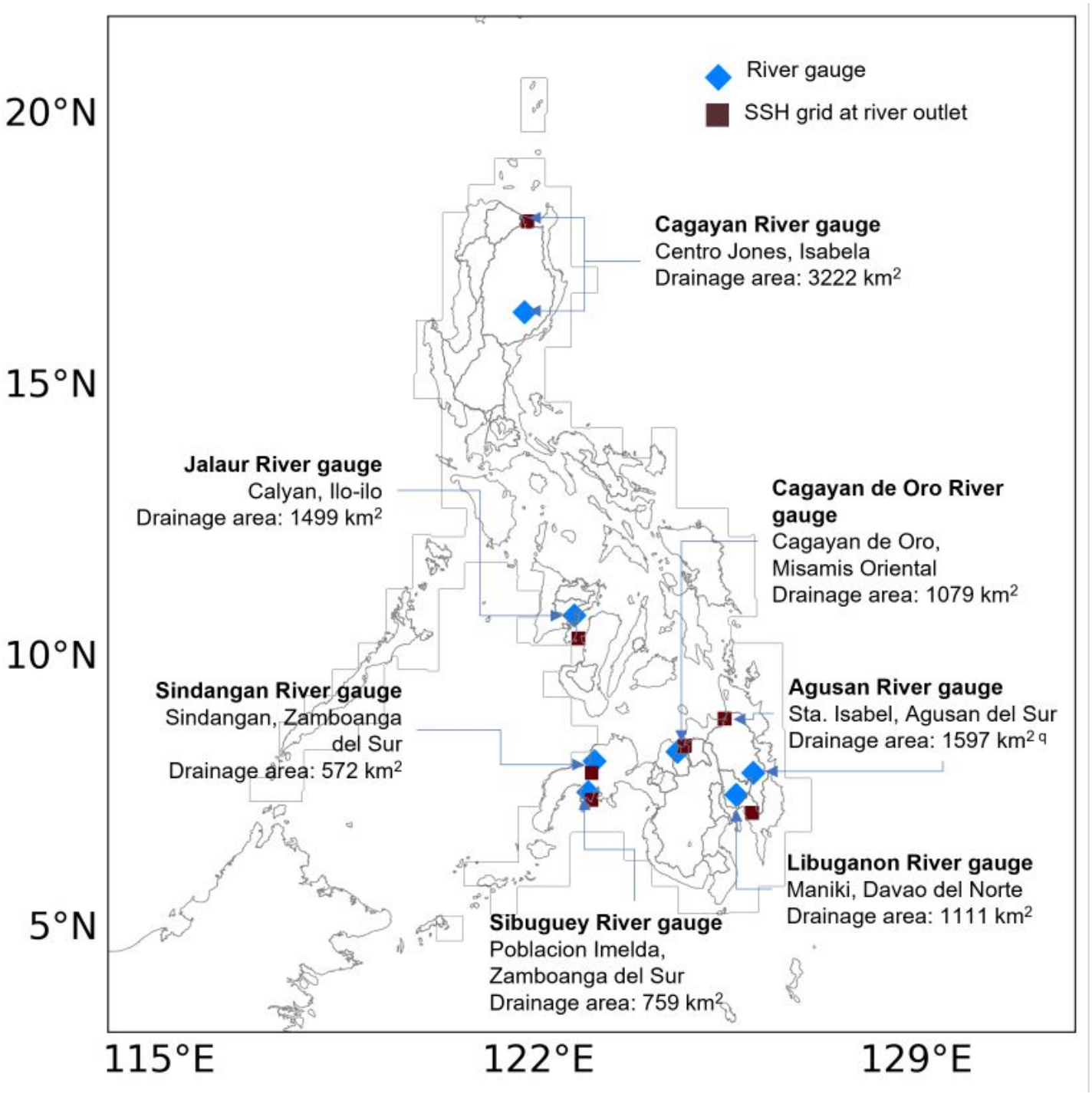

Figure 1

Location of the seven river basins analyzed in this study including where the actual river gauge station is located as well as each river's outlet to the ocean. The thin, gray lines bordering the coastal waters of the country correspond to the spatial overlap of the SSH and GRUN datasets.

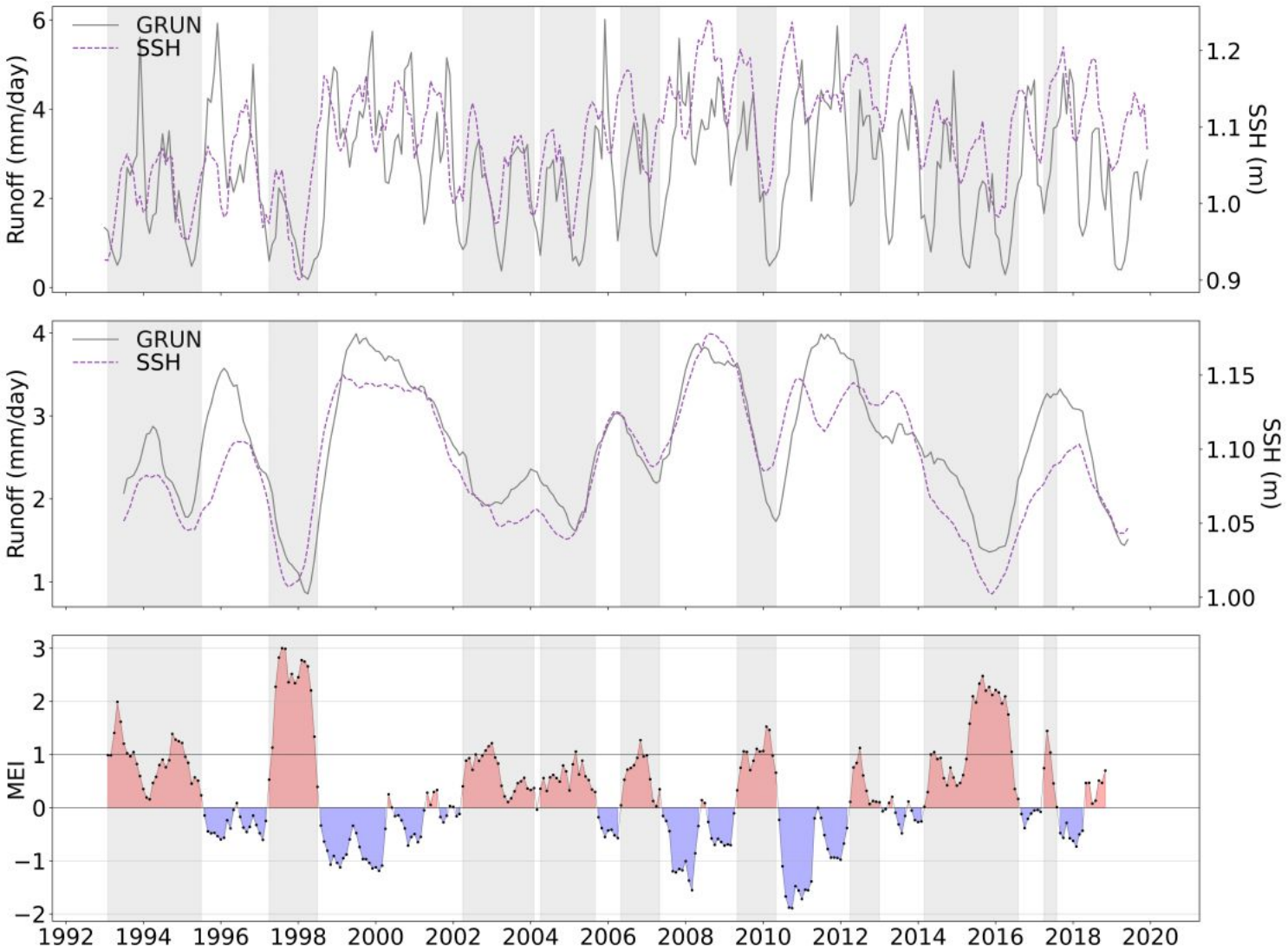

Figure 2

Monthly time series of GRUN and SSH, national means during periods of overlap (1993 - 2019) and the Multivariate ENSO Index (1993 - 2018). Top: monthly time series of GRUN and SSH; middle: deseasonalized and detrended time series of GRUN and SSH; bottom: the MEI. Highlighted time periods (in gray) correspond to the nine relatively strong El Niño events (peak MEI > 1) used in the regression analysis. From left to right, these time periods are: (1) 12/1989 to 07/1995, (2) 04/1997 to 07/1998, (3) 04/2002 to 02/2004, (4) 04/2004 to 09/2005, (5) 05/2006 to 05/2007, (6) 05/2009 to 05/2010, (7) 04/2012 to 01/2013, (8) 03/2014 to 08/2016, and (9) 04/2017 to 08/2017.

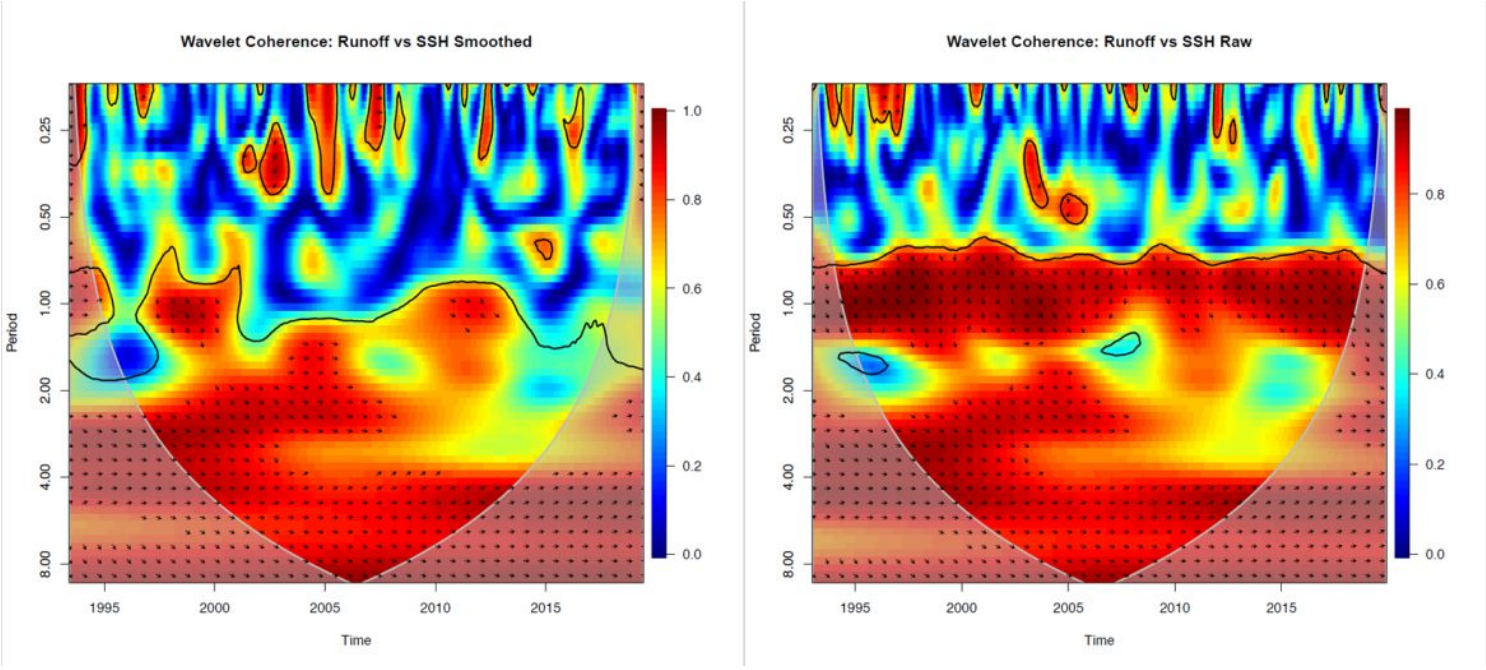

Figure 3

Wavelet coherence plots between runoff and SSH. Direction of arrows indicate time lag; downward direction corresponds to zero time lag, while arrows pointing to the right indicate that SSH leads runoff. Left: Smoothed time series; right: raw time series.

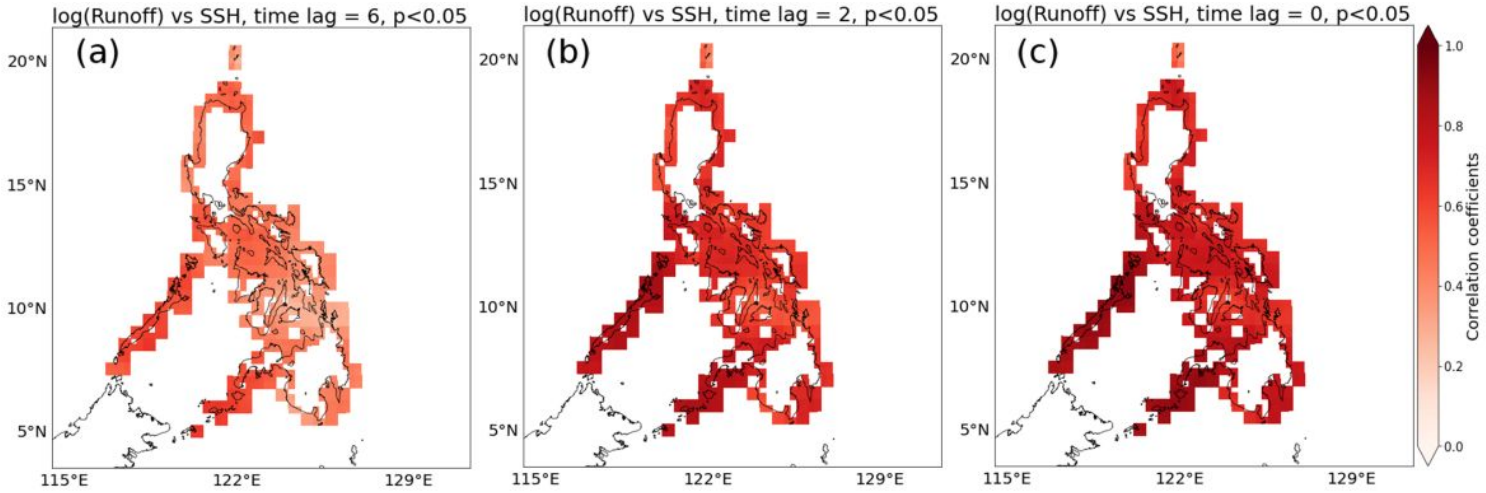

Figure 4

Map of correlation coefficients (1993 - 2019). Left to right: (a) at 6 months that SSH precedes runoff, (b) at 2 months that SSH precedes runoff, (c) at no time lag. Time lag in months.

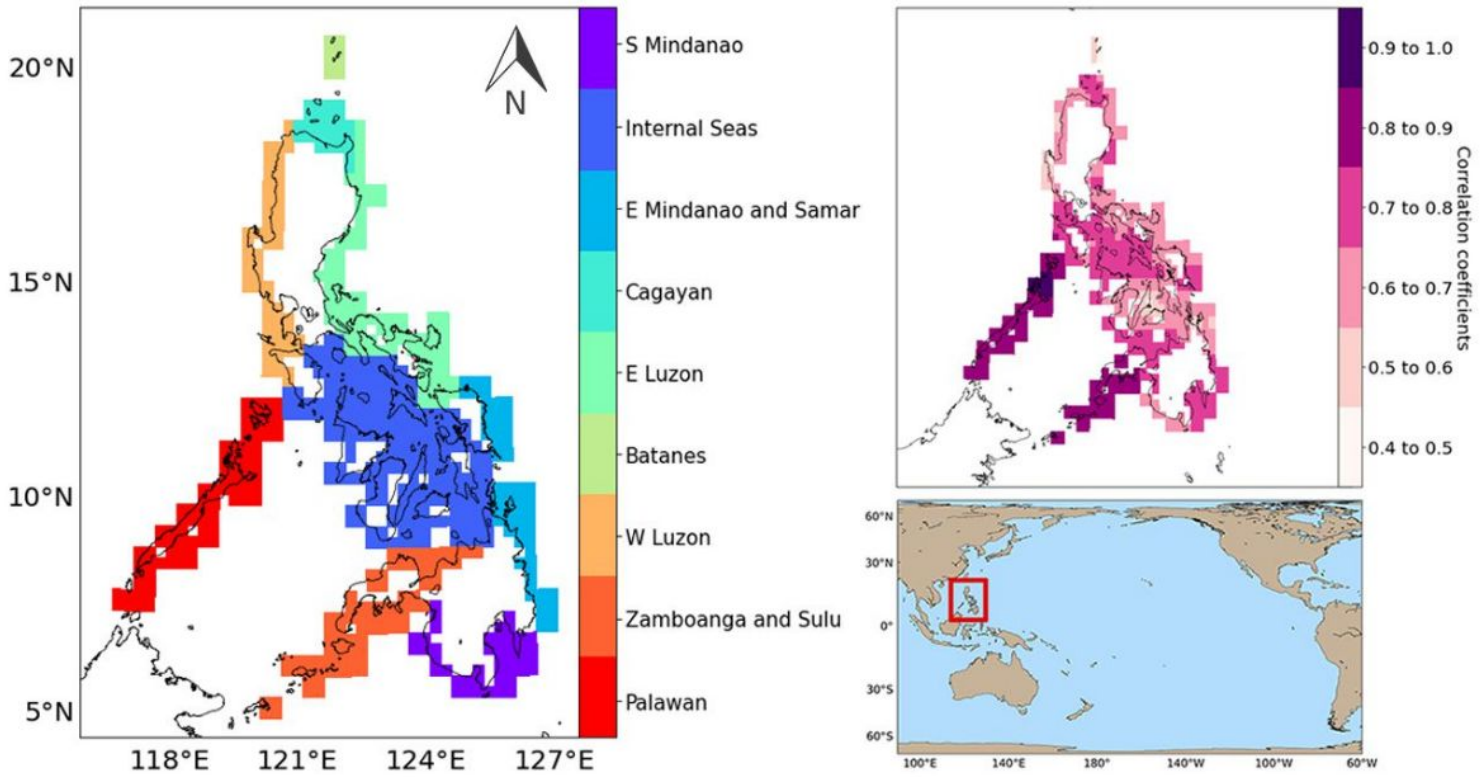

Figure 5

Study area divided per region according to the magnitude of correlation coefficients at -1 month time lag. Right: identified regions; left: reference correlation map at 1 month time lag of SSH and the Pacific Ocean map. Red box indicates the location of the study area.

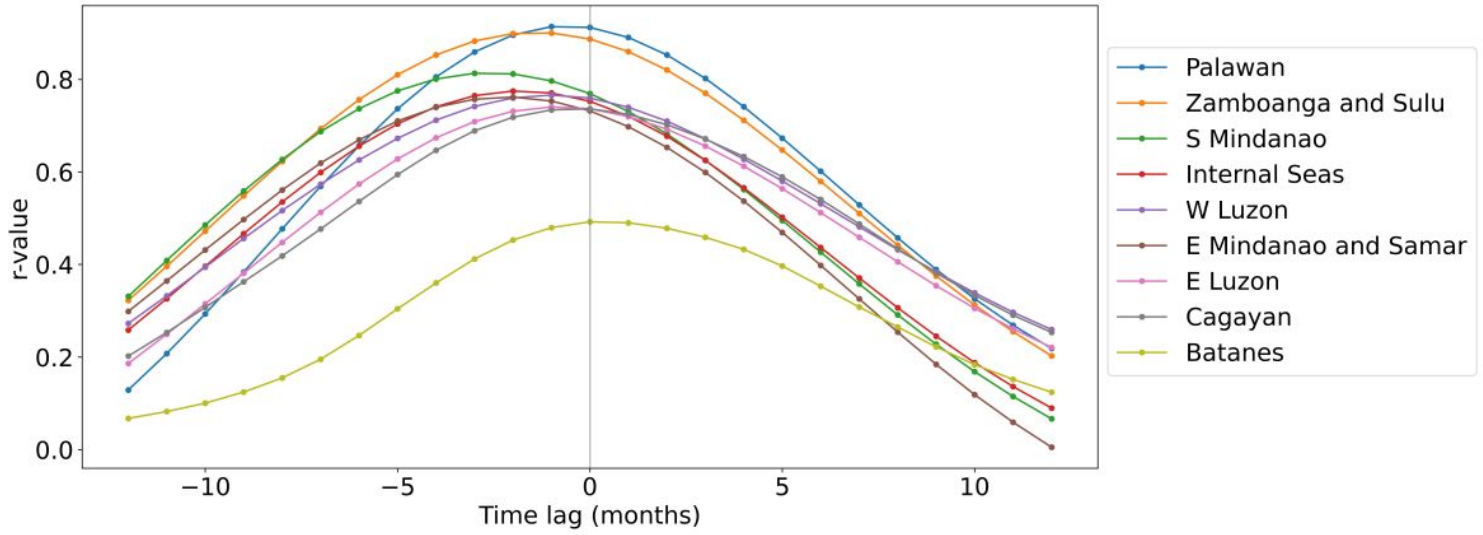

Figure 6

Correlation coefficients between log10(runoff) and SSH at each region from -12 to 12 months of time lag of SSH. The regions are listed in the plot legend according to the magnitude of correlation coefficients calculated; Palawan and Batanes have the highest and lowest peak r-values, respectively. A positive time

lag means SSH precedes runoff; a negative time lag means SSH leads runoff. See Supplementary Table 1 for the matrix of values plotted here.

Supplementary Files

This is a list of supplementary files associated with this preprint. Click to download.

- SuppTable1.pdf